Effect of Blending with Poly(ethylene oxide) on the Dynamics of Poly(methyl methacrylate): A Quasi-Elastic Neutron Scattering Approach

Victoria García Sakai, Chunxia Chen, and Janna K. Maranas*

Department of Chemical Engineering, The Pennsylvania State University, University Park, Pennsylvania 16802

Zema Chowdhuri

NIST Center for Neutron Research, Gaithersburg, Maryland 20899, and Department of Materials Science and Engineering, University of Maryland, College Park, Maryland 20742

Received February 6, 2004; Revised Manuscript Received September 28, 2004

ABSTRACT: The mobility of poly(methyl methacrylate) [PMMA] in a blend with 20 wt % poly(ethylene oxide) [PEO] is assessed using quasi-elastic neutron scattering (QENS) and compared to pure PMMA. The primary conclusion is that the change in dynamics of PMMA, upon blending with PEO, is solely a result of the shift in T_g. Although relaxation times of PMMA are smaller in the blend than in pure PMMA at a given temperature, they collapse onto a single curve when the difference in T_gs is taken into account. Relaxation times are Arrhenius in temperature throughout most of the data, with an activation energy consistent with that observed in dielectric spectroscopy for the merged $\alpha\beta$ process. At temperatures less than $\sim 1.2T_g$, the data suggest that at large spatial scales relaxation times grow in excess of Arrhenius temperature dependence, whereas at small spatial scales Arrhenius behavior continues. The approximate dividing point for this behavior is the static structure peak of PMMA.

Introduction

Polymer systems show complex dynamics and the wide variety of motions observed span an extensive range of time scales. Faster dynamics include not only rotations and vibrations but also side-group motions and local rearrangements involved in the so-called secondary or β-relaxation process.[1] The α-relaxation comprises slower motions involved with the glass transition, typically associated with relaxations of the chain backbone. Changes in both processes when a polymer is incorporated in a miscible blend have been the target of many investigations.

In this work we consider one such miscible blend: poly(methyl methacrylate) [PMMA] and poly(ethylene oxide) [PEO]. This blend exists as a single amorphous phase for concentrations of PEO not greater than 30 by weight. From a thermodynamic point of view, minimal interactions are present, with the Flory−Huggins interaction parameter close to zero as determined by small-angle neutron scattering.[2,3] Dynamic measurements on PEO/PMMA blends using nuclear magnetic resonance [NMR][4−8] and other experimental techniques[9−12] indicate two dynamic responses, which are expected due to the large T_g contrast (around 180 K). Oscillatory shear rheometry[10] has shown that time−temperature superposition fails for this blend. Colby[10] also reported that in blends containing 20% and 30% PEO, if considered at the same $(T - T_g)$, PMMA relaxes slower in the blend than in pure PMMA, while PEO relaxes faster. A study by Lartigue and co-workers[7] using proton NMR reports that the mobility of PEO is highly reduced by the presence of PMMA but remains mobile at temperatures below the glass transition of the blend. More recently, Lutz and co-workers[5] reported that the segmental dynamics of d_4PEO are 12 orders of magnitude faster than PMMA segmental dynamics for a blend containing 3% PEO at temperatures close to the blend T_g. Finally, results from dielectric spectroscopy suggest that the merged $\alpha\beta$-relaxation of PMMA becomes faster when adding PEO.[9]

The complex dynamic behavior exhibited by this blend is common in other blend systems, as observed with a number of experimental techniques: dielectric spectroscopy [DS],[9,13,14] quasi-elastic neutron scattering [QENS],[13,15−17] NMR,[5,13,18] fluorescence anisotropy decay,[20] and dynamic mechanical measurements.[21,22] This scenario has been identified typically for blends where the two components have very dissimilar glass transition temperatures:[13,15,16] PEO and PMMA represent an extreme case as the difference is around 180 K. Theories that attempt to explain these observations are generally based on the idea that each component in the blend experiences an effective local composition different from the bulk composition. Two theories are proposed for explaining the origin of these local environments: (1) *concentration fluctuations* that occur in mixtures and depend on the interactions between the two components and on their molecular weights[18,19,22−24] and (2) *chain connectivity effects,*[18,25] i.e., each component's environment is rich in itself because it is connected to segments of its own kind. The latter model, in which the revelant temperature and composition independent length scale is the Kuhn length, explains dynamic differences in a number of blend and copolymer systems.[26] The model has also been tested on both components of the PEO/PMMA blend.[5,26] With respect to terminal dynamics, the success of the model for the high-T_g component (PMMA) depends on the composition range considered: success is found for PMMA-rich (80%) but not PEO-rich (20−

* To whom all correspondence should be addressed. E-mail: jmaranas@psu.edu.

10.1021/ma0497355 CCC: $27.50
Published on Web 11/25/2004

Table 1. Characterization Results for PMMA Samples

polymer	M_w (kg/mol)	M_w/M_n	T_g (K)
hPMMA	355	1.03	397
d_4PEO	460	1.44	211
hPMMA/d_4PEO			345

60%) blends. Terminal dynamics for the low-T_g component [PEO] have not been tested. For segmental dynamics, only PEO in PMMA rich blends has been tested, and the model is unable to correlate the data.

In this work we concentrate on the segmental mobility of PMMA for which very limited data exist. We compare the mobility of PMMA in the blend with that in pure PMMA using QENS. Because of the difference between the incoherent scattering cross sections of hydrogen (80.27×10^{-24} cm^2) and deuterium (2.05×10^{-24} cm^2), it is possible to highlight the dynamic response of PMMA by deuteration of PEO, without substantially changing the nature of the samples. It is important to recognize that selective deuteration can affect the phase diagram of miscible polymer blends.[27] This could alter concentration fluctuations and potentially the dynamic behavior, although the estimate of contributions from concentration fluctuations to mean dynamic properties is less than ~20% at $T_g + 10$ K.[28] QENS measurements probe short time scales (between 0.1 and 10 ns) and provide spatial resolution over molecular and segmental length scales (3.7 and 10.2 Å).

Our main finding is that the dynamics of PMMA in blends with PEO qualitatively resemble those of pure PMMA. When the change in glass transition temperature on blending is taken into account, results collapse to a single curve, indicating that segmental mobility on short time scales is controlled solely by distance from T_g.

Experimental Section[51]

Sample Preparation. Two polymers were used for the experiments: hydrogenated poly(methyl methacrylate) [hPMMA] and perdeuterated poly(ethylene oxide) [d_4PEO]. Both polymers have narrow molecular weight distributions and were purchased from Polymer Standards Service. The calorimetric glass transition temperatures were measured using a TA Instruments Q1000 differential scanning calorimeter [DSC] on samples of 10−15 mg. The T_g values were calculated from the midpoint of DSC scans at 10 K/min. Both characterization results from gel permeation chromatography and T_g values are given in Table 1.

A blend of hPMMA/d_4PEO containing 20 wt % PEO was prepared by dissolving the two polymers in chloroform and casting them from solution. The blends were kept in a vacuum oven at 340 K for a week to ensure complete removal of the solvent. To ensure that no PEO crystallinity was present initially or occurred during the experiment, DSC scans were run on the blend at 10 K/min, before and after the neutron measurements were undertaken. The scans, indicating a single broad glass transition around of 345 K, were identical. To set the upper temperature limit for the experiments, we ran DSC scans on both hPMMA and d_4PEO in which the temperature was raised from room temperature to 650 K. The scans show degradation at 583 K for hPMMA and 572 K for d_4PEO, based on which we set an upper limit of 530 K for our measurements.

Neutron Scattering Measurements. QENS experiments were performed using the NG2 high-flux backscattering spectrometer (HFBS[29]) at the NIST Center for Neutron Research in Gaithersburg, MD. In this high-energy resolution spectrometer the neutrons are Doppler shifted about an incident wavelength of 6.27 Å, thus providing a range of incoming neutron energies. The neutrons hit the sample and are scattered. The samples which are annular in shape were held in a thin-walled aluminum can mounted on a closed cycle refrigerator unit. The thicknesses of the sample films were ~0.10 mm and were chosen to achieve transmissions of ~90% and minimize multiple scattering effects. An array of detectors receive only those scattered neutrons with a particular final energy, as determined by multiple analyzers. The instrument was operated at two dynamic ranges (energy transfer): ±11 and ±20 μeV. The resolutions (full width at half-maximum) of the spectrometer were 0.80 and 0.87 μeV, respectively, determined by measuring with a vanadium sample at 293 K at each energy transfer range. The momentum transfers (Q) measured ranged between 0.6 and 1.7 Å^{-1}, corresponding roughly to 3−11 Å. The data were grouped in 10 bins with midpoints of 0.62, 0.75, 0.87, 0.99, 1.11, 1.22, 1.42, 1.51, 1.60, and 1.68 Å^{-1}. The raw data were treated by normalizing to monitor and correcting for absorption effects and detector efficiency using software developed by NIST (Data Analysis and Visualization Environment).[30] QENS spectra were obtained at temperatures between 300 and 530 K, encompassing the T_g of the blend and that of pure PMMA.

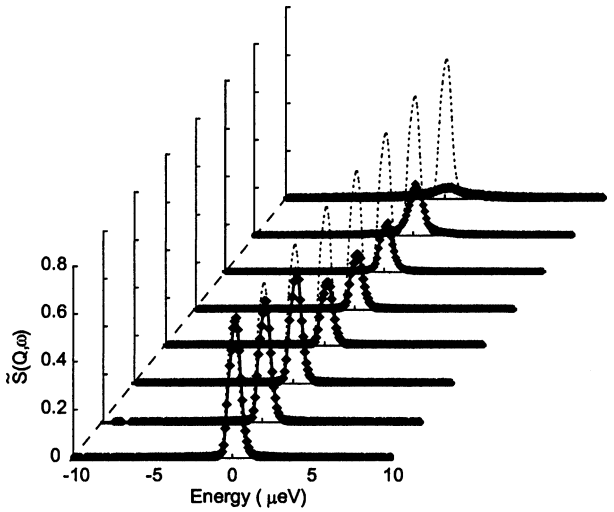

Figure 1. Influence of temperature on QENS spectra for PMMA in a 20% blend at a constant momentum transfer of 0.99 Å^{-1}. The spectra correspond to data at 308, 348, 372, 387, 405, 420, 440 and 490 K, from front to back. The instrumental resolution is shown in each case for comparison (dotted line).

As previously mentioned, the difference in incoherent cross sections between hydrogen and deuterium allows highlighting the motion of one component in the blend by deuterating the other. This is a consequence of the scattering being dominated by the incoherent signal from the hydrogen atoms. The total scattering cross section of the blend sample consists of the sum of the scattering cross sections of all the atoms, those in the hydrogenated component (in this case PMMA) plus those in the deuterated component (PEO). The total scattering cross section includes both incoherent and coherent contributions. Therefore, we can write $\sigma^{total} = \sigma^{PMMA} + \sigma^{PEO} = \sigma_{inc}^{PMMA} + \sigma_{coh}^{PMMA} + \sigma_{inc}^{PEO} + \sigma_{coh}^{PEO}$. We can then calculate the incoherent contribution of PMMA to the total scattering cross section, i.e., $\sigma_{inc}^{PMMA}/\sigma^{total}$, to be approximately 91%. The same calculation for pure PMMA yields gives an incoherent contribution of 93%.

Results

The quasi-elastic spectra of PMMA in the blend and pure PMMA were measured at a series of temperatures ranging from below to well above the T_g of the samples: hPMMA/d_4PEO spectra were measured at T = 308, 324, 348, 372, 387, 405, 420, 440, and 490 K, and hPMMA spectra were taken at T = 413, 424, 447, 465, 503, and 520 K. The spectra give the incoherent energy-dependent structure factor $\tilde{S}(Q,\omega)$ as a function of energy transfer (μeV, $E = \hbar\omega$), as shown in Figures 1

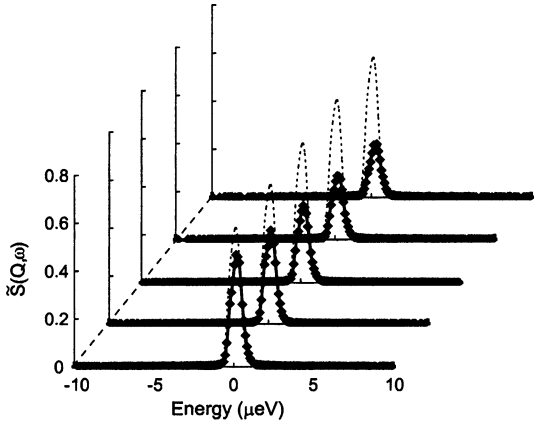

Figure 2. Influence of momentum transfer on QENS spectra for PMMA in a 20% blend at a constant temperature of 420 K. The spectra correspond to data at 0.75, 0.99, 1.22, 1.42, and 1.60 Å^{-1}, from front to back. The instrumental resolution is shown in each case for comparison (dotted line).

and 2 for PMMA in the blend. Also shown in the figures is the instrumental resolution. We use a tilde to differentiate the "measured" dynamic structure factor [$\tilde{S}(Q,\omega)$] from the "true" dynamic structure factor of the sample [$S(Q,\omega)$], which has the instrumental resolution removed. In the first of these figures the spectra are shown as the temperature is increased from below to above the blend T_g. As motion becomes faster with increasing temperature, the peaks become shorter and broader and stop resembling the resolution spectra. A similar broadening is observed as the value of Q is increased while keeping the temperature constant. This is shown in Figure 2. The line shape of the spectra in both figures consists of the superposition of at least two peaks, a tall and thin Gaussian peak and either one or a number of shorter and wider peaks. The Gaussian peak corresponds to the elastic contribution to the scattering function, i.e., to scattering events in the absence of motion. The broad peak corresponds to the quasi-elastic scattering that results from the mobility of the scattering centers.

The dynamic structure factors of pure PMMA and PMMA in the blend are compared in Figure 3. The scattering intensity has been normalized by the maximum scattering intensity for the comparison. The plots contain data at $Q = 0.62$ Å^{-1} and at temperatures $T =$ 490 K (PMMA in the blend) and 503 K (pure PMMA). Blending significantly increases the broadening of the spectra, implying that PMMA moves considerably faster in the blend as compared with the pure state, if compared at the same temperature. If compared at the same distance above T_g, as shown in Figure 4, very little difference is observed.

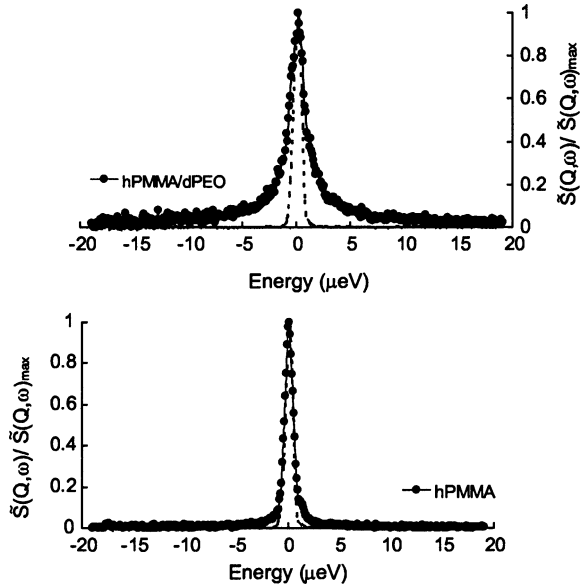

Figure 3. Effect of blending on the QENS spectra of hPMMA at approximately the same temperature ($T = 503$ K for pure PMMA and 490 K for hPMMA/d$_4$PEO). In both cases results are shown for a momentum transfer of 0.62 Å^{-1}. The spectra have been normalized to the maximum intensity and are compared to the instrumental resolution.

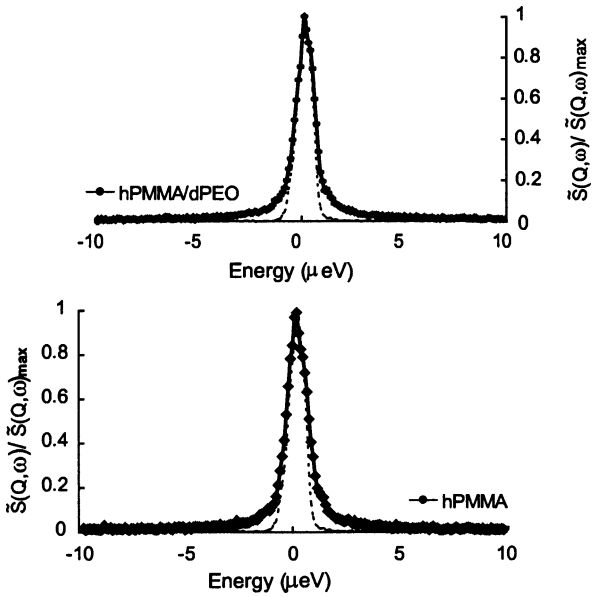

Figure 4. Effect of blending on the QENS spectra of hPMMA at a temperature the same distance above the glass transition temperature (T_g + 95 K) and at $Q = 0.62$ Å^{-1}. The spectra have been normalized to the maximum intensity and are compared to the instrumental resolution.

Data Analysis and Evaluation

Figure 4 suggests that the mobility of PMMA is invariant if considered at the same distance above T_g. To make a numerical comparison, the data are fit with the empirical Kolrausch−Williams−Watts[31] (KWW) equation:

$$\frac{S(Q,t)}{S(Q,0)} = A(Q,T)\exp\left[-\left[\frac{t}{\tau_{KWW}(Q,T)}\right]^{\beta(Q,T)}\right] \quad (1)$$

where $S(Q,t)$ is the intermediate scattering function at time t, $S(Q,0)$ is the intermediate scattering function at time $t = 0$, $A(Q,T)$ is a prefactor, τ_{KWW} is the characteristic relaxation time, and β is the stretching exponent. In analyzing the data in this way, we assume they can be described by the KWW functional form. This is reasonable given that in the neat state and in blends[13,15,16,32−34] the KWW equation describes the time decay of all polymers, even at temperatures well above T_g. At short time scales (less than 1 ps), a simple exponential process appears, but the backscattering spectrometer does not have sufficient dynamic range to observe this.

The intermediate scattering function $S(Q,t)$ is the Fourier transform (FT) in the time domain, of the true

dynamic structure factor $S(Q,\omega)$, which is in the frequency domain. The data are fit in the time domain because there is no analytical transform of the KWW equation in the energy domain (except for $\beta = 0.5$) and because any small differences in $S(Q,\omega)$ are magnified in $S(Q,t)$. The spectra are Fourier transformed by directly applying the discrete complex Fourier integral to each set of measured constant temperature and momentum transfer results:[35]

$$\tilde{S}(Q,t) = \sum_{k=1}^{N} \tilde{S}(Q,\omega_k) \exp(-i\omega_k t)\Delta\omega_k \qquad (2)$$

In the expression above, k represents a data point and N the total number of data points, ω_k is the angular frequency ($= E_k/\hbar$, where E is the energy), and $\Delta\omega_k$ is the width of the frequency interval between data points. The measured dynamic structure factor $\tilde{S}(Q,\omega)$ includes the true dynamic structure factor $S(Q,\omega)$ convoluted with the resolution function of the instrument $R(Q,\omega)$. Applying the FT converts the convolution into a multiplication in the time domain:

$$\tilde{S}(Q,\omega) = S(Q,\omega) \otimes R(Q,\omega) \qquad (3)$$

$$\Updownarrow$$

$$\tilde{S}(Q,t) = S(Q,t) \times R(Q,t) \qquad (4)$$

Therefore, the resolution can be removed by simply dividing the FT of the spectra by the FT of the resolution function.

Once $S(Q,t)$ and $S(Q,0)$ are calculated, the intermediate scattering functions are fit with the KWW equation. The intermediate scattering functions for PMMA in the blend are shown in Figure 5 as a function of temperature and momentum transfer. As expected, mobility increases with increasing T and Q. The lines represent the best fit to the KWW equation using the procedure described below. The limited time window of the backscattering instrument and the stretched nature of the relaxation result in small decays particularly at low temperatures and small Q values. To address this difficulty, we link the fits with more decay (those at high T and Q) to those with less decay by fitting all the data simultaneously and requiring that the parameters do not behave unphysically; for example, relaxation times should not increase with increasing temperature. This allows the data with small decays to benefit from data which is more certain. It should be noted that even with this fitting procedure, the data at the lowest temperatures do not decay enough and are discarded. Thus, although we provide a fit for $T = 348$ K in Figure 5, the resulting parameters are too uncertain and are excluded from subsequent analysis.

The fitting is accomplished using a nonlinear optimization solver CONOPT, accessed via the general algebraic modeling system (GAMS). We minimize the squared difference between predicted and measured values of $S(Q,t)/S(Q,0)$. The result is a full set of parameters $A(Q,T)$, $\beta(Q,T)$, and $\tau(Q,T)$. The mathematical formulation of the problem is included as Supporting Information. The following constraints are used: (1) Relaxation times between 0.0001 and 10^6 ns are allowed. Data sets for which this cannot be satisfied are discarded. (2) Relaxation times increase with decreasing temperature, i.e., the lower the temperature the slower the motion. (3) Relaxation times decrease with increasing Q (compared with collective relaxation times which show modulation with the static structure factor $S(Q)$, i.e., de Gennes narrowing).[36,37] (4) A increases with decreasing temperature and length scale—the smaller the value of A, the greater the fraction of the motion faster than the instrumental time window; this dependence for incoherent scattering has also been observed by other authors.[37,38]

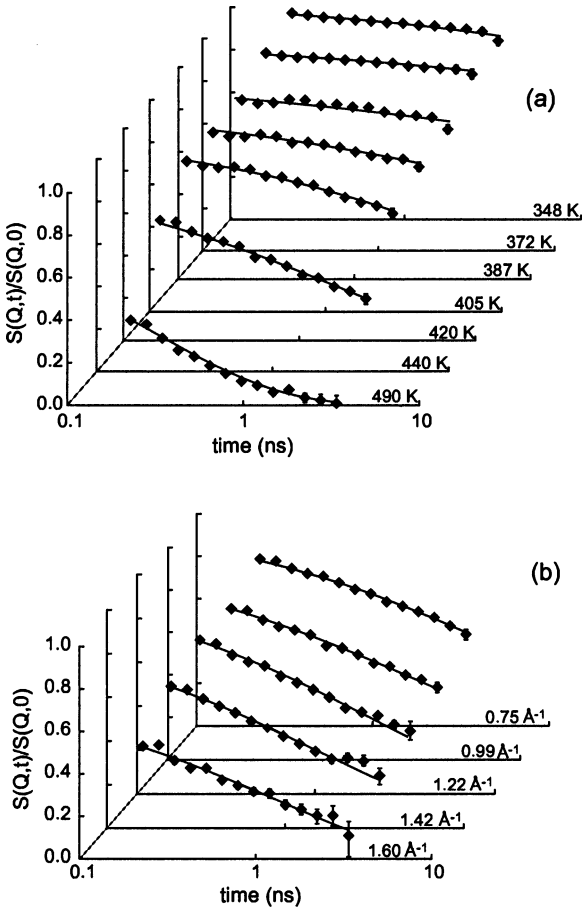

Figure 5. Intermediate scattering function $S(Q,t)/S(Q,0)$ of PMMA in the blend with 20% PEO as a function of (a) temperature at a constant $Q = 0.99$ Å^{-1} and as a function of (b) momentum transfer at a constant $T = 440$ K. The curves are fits obtained using the KWW equation. Error bars correspond to the maximum, and minimum values of $S(Q,t)/S(Q,0)$ are calculated as explained in the Data Analysis section.

Because of the large number of fitting parameters (three) that are often closely coupled, we wish to set an error bar that will represent the maximum range of each parameter that can adequately represent the data. Error bars for the Fourier transformed data as well as for the KWW parameters are calculated using a sampling technique. This involves randomly generating a large number of possible data sets with each data point randomly placed within its error bars. To study the effect of sample number, the number of generations was varied from 100 to 5000. The size of the error bars did not change beyond that for 500 generations. Thus, this was chosen as the sampling quantity. The error bars presented in the figures correspond to the maximum and minimum values of each parameter obtained in the 500 fits and thus represent the range of each parameter that can provide a good fit to the data. Values outside the error bars cannot provide a reasonable fit regardless of the values of the other two parameters.

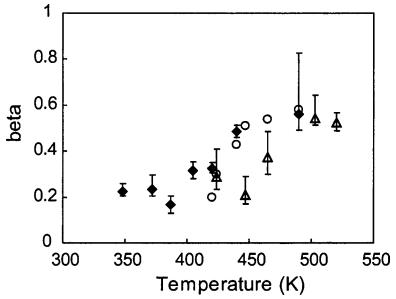

Figure 6. Comparison of stretching exponent values obatined from QENS and dielectric spectroscopy[39] at $Q = 0.62$ Å^{-1}: solid diamonds, PMMA in the blend from this work; open circles, pure PMMA data from dielectric spectroscopy; triangles, pure PMMA from this work.

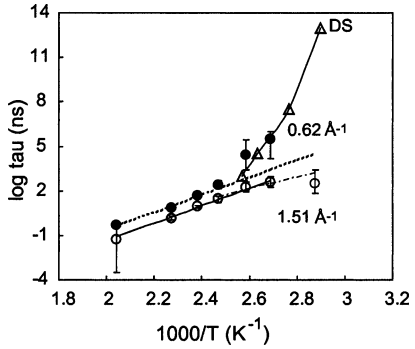

Figure 7. Temperature dependence of relaxation times of PMMA in the blend at two spatial scales: 0.62 and 1.51 Å^{-1}. Lines represent fits using the Arrhenius equation, eq 5: dotted line, fit to $Q = 0.62$ Å^{-1} data excluding the lowest two temperatures; solid line, fit to $Q = 1.51$ Å^{-1} data excluding the lowest temperature; broken line, fit to $Q = 1.51$ Å^{-1} data excluding the highest three temperatures. Triangles show data from dielectric spectroscopy[39] for the α-relaxation of pure PMMA shifted by T_g.

The validity of the fitting procedure is tested using the stretching exponent β as it is the most difficult parameter to assign. We choose to test it with data at $Q = 0.62$ Å^{-1} since it is the smallest momentum transfer measured and has the smallest decays. Figure 6 shows β values for pure PMMA and PMMA in the blend obtained from QENS, as well as values obtained for the α-relaxation of pure PMMA from dielectric spectroscopy[39] where the large dynamic range provides full decays and a much better assignment of β. The values obtained from QENS and DS for pure PMMA are very similar, indicating that the fitting procedure is returning reasonable results.

Dynamics of PMMA in the Blend. In what follows, the temperature and momentum transfer dependence of τ and β are addressed [A is very close to 1.0 in all fits]. Relaxation times of PMMA in the blend are plotted as a function of temperature at representative low and high Q values in Figure 7. At high temperatures, relaxation times increase with decreasing temperature following an Arrhenius behavior

$$\tau = \tau_0 \exp\left(\frac{E_a}{kT}\right) \tag{5}$$

where the activation energy is 110 kJ/mol, consistent with the αβ process of pure PMMA.[39] This process is observed at all spatial scales. As the temperature is decreased, a split is observed. Although this involves our most uncertain points, the data suggest that, at low Q, Arrhenius behavior is no longer obeyed. This change in temperature dependence appears to agree with the α-relaxation of pure PMMA[39] also shown in Figure 7. The latter data are shifted by $T - T_g$ for comparison with the blend data.

Divergence from Arrhenius behavior is only observed at Q values smaller than the first peak in the static structure factor for pure PMMA.[40] A similar result has been observed for pure polybutadiene,[41] where at intermolecular spatial scales {Q less than Q_{max}, the position of the first peak in $S(Q)$} relaxation times follow the temperature dependence of the α-relaxation, but at momentum transfers higher than this, relaxation times exhibit an Arrhenius temperature dependence characteristic of the β-relaxation. Although the data for polybutadiene represent collective motion where the connection between static structure factor and dynamics is clear, this structure also has some bearing on self-motion. The spatial scale in a neutron experiment acts as a magnifying glass with varying power. The incoherent experiment follows the motion of protons within subvolumes of size specified by the momentum transfer. If the subvolume is small enough (high Q), it will focus on protons within single PMMA chains, with diminished probability of other chains in the surrounding area (specified by Q). Certainly the probability is reduced significantly below the intermolecular peak in $S(Q)$, which for PMMA is centered at 0.9 Å^{-1} and has a width of 1 Å^{-1}. At present there is no data on $S(Q)$ for the blend, but since our measurements probe the dynamics of PMMA, a comparison with pure PMMA is relevant. We can thus associate the low Q data in Figure 7 with regions that contain atoms in other chains (intermolecular spatial scales $Q < Q_{max}$) and the high Q data with regions likely to view a single chain average (intramolecular spatial scales). The terms "intermolecular" and "intramolecular" represent the dominant contribution to the subvolumes surrounding the observed protons at the specified spatial scale and not to specific separations between pairs of atoms. As with polybutadiene, relaxation times at intermolecular spatial scales show indication of a rapid increase with decreasing temperature. Deviations from Arrhenius behavior are systematic with the lower two temperatures deviating outside of the error. With our assignment of error, this means that smaller relaxation times cannot describe the data regardless of the values for A and β. The same activation energy describes all spatial scales at high temperatures, including the intramolecular scale in Figure 7 ($Q = 1.51$ Å^{-1}). This is shown with the solid line which has the same activation energy of 110 kJ/mol, fit through all but the lowest temperatures (the best fit gives $E_a = 116$ kJ/mol). The data at this high Q is also suggestive of a change in slope as T_g is approached; therefore, another fit is made using only temperatures very close to T_g. The activation energy for this process is 78 kJ/mol. This change in slope has also been observed in pure PMMA by Bergman and coworkers, who report an activation energy of 79.4 kJ/mol near T_g. As a final comment, the data suggest that the merger of these processes which resemble the α- and β-processes in pure PMMA occurs near $1.15T_g$, which is consistent with other glass formers.

We now discuss the spatial scale dependence of the characteristic relaxation times of PMMA in the blend. Figure 8 shows a plot of relaxation times vs Q at four

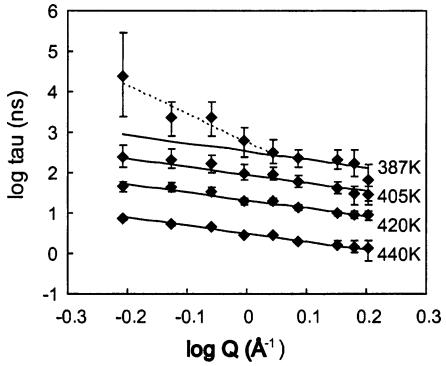

Figure 8. Q dependence of the characteristic relaxation times obtained for PMMA in the blend at four different temperatures. Lines are fits using eq 6 with $n = 2$ (solid) and $n = 2/\beta$ (dashed). The vertical dashed line shows the spatial scale of the peak in $S(Q)$ for pure PMMA.

temperatures. The solid lines represent fits using a power law:

$$\tau_{KWW}(Q,T) \propto Q^{-n} \tag{6}$$

In the case of pure polymers, n values of 2 and $2/\beta$ have been observed.[36,42−44] Most of the present data can be described with an exponent of −2 throughout the measured spatial range. This scaling indicates Gaussian dynamics. At temperatures ≤372 K the data suggest the appearance of a second regime with a scaling of $-2/\beta$ at spatial scales smaller than $Q = 1.1$ Å^{-1}. Unfortunately, this involves the data with the largest errors, precluding a definite statement. The data are more consistent with a crossover in slope than with a continuation of −2 scaling (also shown in Figure 8). The possibility of a $-2/\beta$ scaling appears at length scales large enough to include significant intermolecular contributions and at temperatures less than $1.15T_g$. For pure polymers, a crossover has been observed with both experiments[36,45] and molecular dynamics simulations.[46] For simple liquids, −2 scaling indicates a Gaussian form of the single particle displacement. This normally occurs at short (ballistic motion) and long (free diffusion) time scales. In polymers, a sublinear dynamic regime occurs at intermediate time scales—comparable to those probed by QENS. In this regime, the Gaussian form leads to a $-2/\beta$ scaling. In the molecular dynamics simulations of Colmenero et al.,[46] the authors show that a −2 scaling emerges with a deviation from Gaussian behavior as Q becomes larger than Q_{max} (the "intermolecular" peak in the static structure factor). This is consistent with our results at low temperature. The persistence of a −2 scaling at high temperatures suggests that particle displacements are not Gaussian throughout our temperature range, but one would expect (and the work by Colmenero et al.[46] confirms) that as the temperature is raised Gaussian behavior is eventually recovered for all Q. One possible reconciliation is that the spatial scale of the crossover is temperature-dependent, specifically shifting to lower Q and moving out of the window of the backscattering spectrometer. The temperature dependence reported in the work of Farago and coworkers[36] is not pronounced and does not support such a conclusion. One must also remember that the current system is a miscible blend which may introduce additional aspects not present in pure polymers. A change from −2 to $-2/\beta$ has also been associated with a change from heterogeneous to homogeneous dynamics.[45] This explanation is inconsistent with our data since spatial heterogeneities would be expected to become more prominent near T_g.[37,47−49]

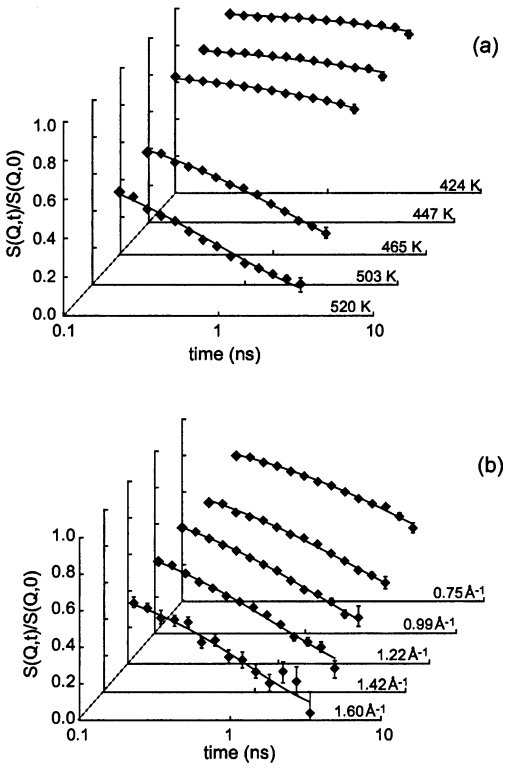

Figure 9. Intermediate scattering function $S(Q,t)/S(Q,0)$ of pure PMMA at (a) a constant momentum transfer of 0.99 Å^{-1} and different temperatures and (b) a constant temperature of 503 K and different momentum transfers. The lines are fits using the KWW equation. Error bars correspond to the maximum and minimum values of $S(Q,t)/S(Q,0)$ calculated as explained in the Data Analysis section.

A physically appealing scenario would be that at high temperatures and small spatial scales simple diffusion is observed in conjunction with Arrhenius temperature dependence, whereas below $\sim 1.15T_g$ (or the T_g of PMMA) and at spatial scales larger than the interchain spacing for PMMA, sublinear diffusion and Vogel temperature dependence set in. This scenario requires that the relaxation decays exponentially, which is not the case for the present results. Decays for polymers are stretched even at high temperatures and long times.

Comparison with Pure PMMA Dynamics. Our major conclusion results from comparing the blend data with QENS measurements on pure PMMA. The intermediate scattering functions for pure PMMA are shown in Figure 9 at temperatures ranging from 424 to 520 K. Like with the blend data, molecular motion accelerates with increasing temperature and is faster at smaller spatial scales. The scattering functions also show that the temperature where the onset of mobility takes place has been missed; there is a clear break between the decay curves at 465 and 503 K. As a result, the solver fails to find a solution to the problem when given all temperature and Q data simultaneously, and the data are analyzed at each temperature separately. This means that only the Q-dependent constraints are applied, i.e., inequalities (12) and (14) [see Supporting Information].

Relaxation times are plotted in Figures 10 and 11 as a function of temperature for pure PMMA and PMMA in the blend. The comparison is made at the same two

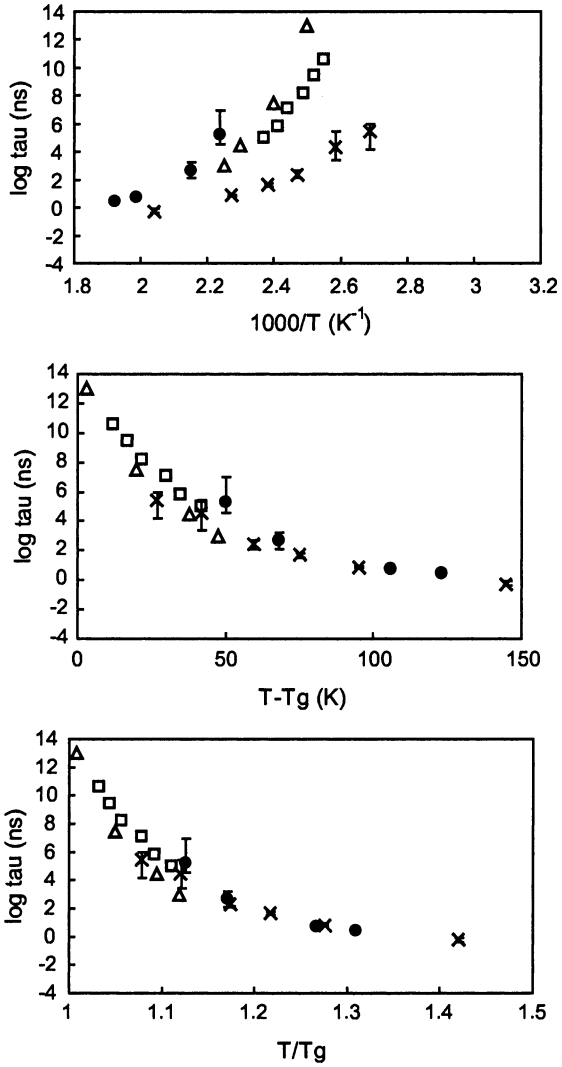

Figure 10. Effect of blending on relaxation times for PMMA at $Q = 0.62$ Å^{-1}. The top figure shows a comparison at the same temperature, the middle figure a comparison at the same $T - T_g$, and the bottom figure a comparison at T/T_g. In all figures, solid circles represent pure PMMA data from this work, crosses represent data for PMMA in the blend from this work, and open triangles and open squares show data for the α-relaxation of pure PMMA from dielectric spectroscopy[39] and light scattering measurements,[50] respectively.

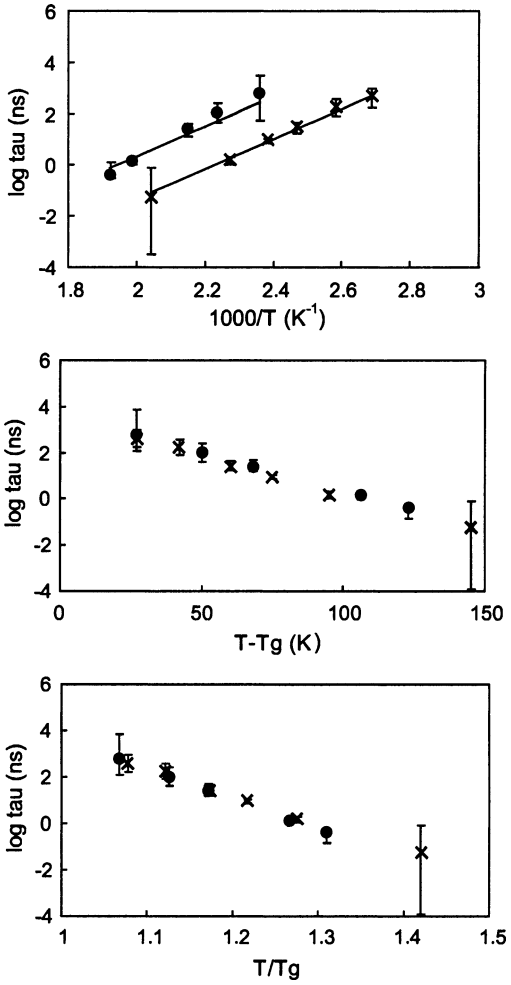

Figure 11. Effect of blending on relaxation times for PMMA at $Q = 1.51$ Å^{-1}. The top figure shows a comparison at the same temperature, the middle figure a comparison at the same $T - T_g$, and the bottom figure a comparison at the same T/T_g. In all figures, solid circles represent the pure PMMA data and crosses represent the data for PMMA in the blend. The solid lines show the Arrhenius temperature dependence of the relaxation times and correspond to an activation energy of 118 kJ/mol.

momentum transfers considered before: 0.62 and 1.51 Å^{-1}. It is apparent that the behavior of PMMA in the blend closely resembles that observed for pure PMMA. At the larger spatial scale, relaxation times increase rapidly as the temperature is decreased toward the glass transition temperature. The neutron data are consistent with the high-frequency end of the α-relaxation of pure PMMA, as illustrated by the dielectric spectroscopy and light scattering data included in the figure. At the smaller spatial scale there is an Arrhenius temperature dependence with an activation energy of 118 kJ/mol for pure PMMA and 110 kJ/mol for the blend—consistent with the merged $\alpha\beta$ process. The similar temperature behaviors suggest that PMMA retains its pure component dynamic characteristics in the blend with a shift in temperature due to the presence of PEO.

To test this, we attempt to collapse the data on a single curve by comparing the data at a temperature the same distance above the glass transition. These comparisons are shown in the middle and bottom plots of the figures. The data now overlap, indicating that the change in the time scale of the α or $\alpha\beta$ processes of PMMA upon blending is solely a result of the change in glass transition temperature due to the addition of PEO. This is consistent with observations on the polyisoprene/poly(vinylethylene)[17,19] where the relaxation rate of the high-T_g component tracks the average T_g of the mixture.

The comparison between the spatial dependence of the relaxation times of PMMA the blend and that of pure PMMA is shown in Figure 12. The behavior of pure PMMA (upper plot) is similar to PMMA in the blend. At high temperature a power law of −2 is observed. As the temperature is decreased, a $-2/\beta$ scaling more closely resembles the data than a −2 scaling. The crossover in Q scalings is located at approximately the same spatial scale ($Q \approx 1.2$ Å^{-1}) and temperature (between $1.12T_g$ and $1.17T_g$) as seen in the blend.

As further evidence for the scaling with distance above T_g, the lower plot shows the spatial dependence of the relaxation times for PMMA in the blend and pure PMMA at the same distance above T_g, $T_g + 65$ K, and $T_g + 100$ K (these being the only two $T + T_g$ values

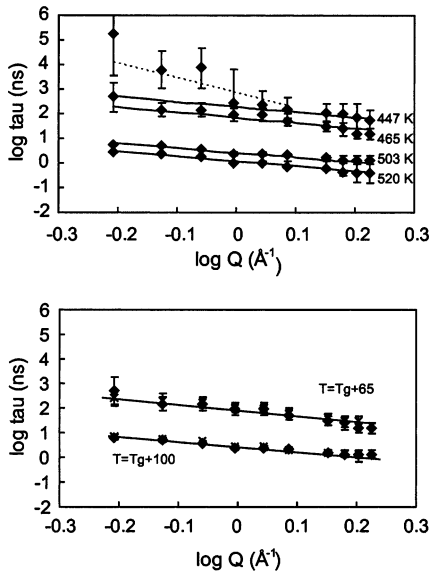

Figure 12. Effect of blending on the spatial dependence of the characteristic relaxation times. The top figure shows the relaxation times obtained for pure PMMA at four different temperatures. Lines are fits using eq 6 with $n = 2$ (solid) and $n = 2/\beta$ (dashed). The bottom figure compares the spatial dependence of the relaxation times for pure PMMA and PMMA in the blend at $T - T_g = 65$ and 100 K (solid diamonds represent the blend data and crosses represent the pure PMMA data). The solid lines are fits using eq 6 with $n = 2$.

common to both systems). In both cases the data coincide again, confirming that the change of dynamics upon blending can be explained by the change in T_g.

As a final comment, we consider the effect of blending on the stretching exponent, i.e., do the dynamic processes observed become broadened upon blending? One might expect that placing PMMA in a blend with PEO will increase the width of the distribution of mean relaxation times (i.e., decrease β) due to concentration fluctuations, but it also renders the system further from T_g which would tend to increase β. In Figure 6, β values were shown for pure PMMA and PMMA in the blend at $Q = 0.62$ Å^{-1}. Values show similar temperature dependencies for both systems; pure PMMA is perhaps slightly broader. If compared at the same distance above T_g (not shown) which eliminates the second effect, our data suggest that the larger range of environments has little effect on the breadth of the relaxations. This would imply that the dynamic behavior of PMMA is insensitive to the effects of concentration fluctuations.

Summary and Conclusions

We have investigated the effect of blending PMMA with PEO using quasi-elastic neutron scattering, at temperatures below and above the glass transition. The measurements cover spatial scales spanning the peaks in the static structure factor of pure PMMA. Despite the complexity of prior results on this system, for PMMA in the PEO/PMMA blend, an adequate description of mean blend relaxation times may be obtained simply by correcting for the difference between $T_{g,PMMA}$ and $T_{g,blend}$. If compared at the same temperature, the motion of PMMA is accelerated by the presence of PEO, but if compared at the same distance above T_g, relaxation times coincide. This observation, although intriguing, is limited by the following. To obtain relaxation times, we assume that the self-intermediate scattering function can be described by a stretched exponential and that an adequate estimation of the stretching exponent is possible given the small time window of the backscattering spectrometer. The latter concern is somewhat alleviated by the fact that we find good agreement between pure PMMA stretching exponents from our fits and those from DS, where a large time window is available. Although it would be preferable to test this agreement for the blend results, such data are not available. One must also appreciate that the observed scaling with T_g is limited to the early stages of relaxation behavior that are observable with QENS. It is certainly possible that this observation does not hold at temperatures approaching T_g. To answer this question, experiments such as DS are required.

For both pure PMMA and PMMA in the blend, Arrhenius behavior and a -2 spatial scaling are observed except at spatial scales greater than interchain spacing and low temperatures where relaxation times suggest a Vogel temperature dependence and a $-2/\beta$ scaling with Q. Confirmation of this result requires incoherent measurements with better resolution, which at present are not possible.

Acknowledgment. Financial support for this work was provided by the National Science Foundation, Polymers Program, through a CAREER Grant DMR-0134910. The authors acknowledge Dr. Anshuman Gupta for help with the GAMS formulation and execution.

Supporting Information Available: Mathematical formulation of the optimization problem used to fit the KWW equation to QENS data. This material is available free of charge via the Internet at http://pubs.acs.org.

References and Notes

(1) Johari, G. P.; Goldstein, M. *J. Chem. Phys.* **1970**, *53*, 2372.
(2) Ito, H.; Russell, T. P.; Wignall, G. D. *Macromolecules* **1987**, *20*, 2213.
(3) Hopkinson, I.; Kiff, F. T.; Richards, R. W.; King, S. M.; Farren, T. *Polymer* **1995**, *36*, 3523.
(4) Schantz, S. *Macromolecules* **1997**, *30*, 1419.
(5) Lutz, T. R.; He, Y.; Ediger, M. D.; Cao, H.; Lin, G.; Jones, A. A. *Macromolecules* **2003**, *36*, 1724.
(6) Straka, J.; Schmidt, P.; Dybal, J.; Schneider, B.; Spevácek, J. *Polymer* **1995**, *36*, 1147.
(7) Lartigue, C.; Guillermo, A.; Cohen-Addad, J. P. *J. Polym. Sci., Part B: Polym. Phys.* **1997**, *35*, 1095.
(8) Schantz, S.; Veeman, W. S. *J. Polym. Sci., Part B: Polym. Phys.* **1997**, *35*, 2681.
(9) Dionisio, M.; Fernandes, A. C.; Mano, J. F.; Correia, N. T.; Sousa, R. C. *Macromolecules* **2000**, *32*, 1002.
(10) Colby, R. H. *Polymer* **1989**, *30*, 1275.
(11) Zawada, J. A.; Ylitalo, C. M.; Fuller, G. G.; Colby, R. H.; Long, T. E. *Macromolecules* **1992**, *25*, 2896.
(12) Fytas, G.; Kanetakis, J.; Floudas, G.; Wang, C. H. *Polym. Commun.* **1990**, *11*, 31.
(13) Cendoya, I.; Alegría, A.; Alberdi, J. M.; Grimm, J. C. H.; Richter, D.; Frick, B. *Macromolecules* **1999**, *32*, 4065.
(14) Alvarez, F.; Alegría, A.; Colmenero, J. *Macromolecules* **1997**, *30*, 597.
(15) Doxastakis, M.; Kitsiou, M.; Fytas, G.; Theodorou, D. N.; Hadjichristidis, N.; Meier, G.; Frick, B. *J. Chem. Phys.* **2000**, *112*, 8687.
(16) Hoffmann, S.; Willner, L.; Richter, D.; Arbe, A.; Colmenero, J.; Farago, B. *Phys. Rev. Lett.* **2000**, *85*, 772.
(17) Doxastakis, M.; Chrissopoulou, K.; Aouadi, A.; Frick, B.; Lodge, T. P.; Fytas, G. *J. Chem. Phys.* **2002**, *116*, 4707.
(18) Chung, C. C.; Kornfield, J. A.; Smith, S. D. *Macromolecules* **1994**, *27*, 5729.
(19) Kumar, S. K.; Colby, R. H.; Anastasiadis, S. H.; Fytas, G. *J. Chem. Phys.* **1996**, *105*, 3777.
(20) Adams, S.; Adolf, D. B. *Macromolecules* **1999**, *32*, 3136.

(21) Yang, X.; Halasa, A.; Hsu, W.; Wang, S. *Macromolecules* **2001**, *34*, 8532.
(22) Roland, C. M.; Ngai, K. L. *Macromolecules* **1991**, *24*, 2261.
(23) Zetsche, A.; Fischer, E. W. *Acta Polym.* **1994**, *45*, 168.
(24) Kamath, S.; Colby, R. H.; Kumar, S. K.; Karatasos, K.; Floudas, G.; Fytas, G.; Roovers, J. E. L. *J. Chem. Phys.* **1999**, *111*, 6121.
(25) Lodge, T.; McLeish, T. C. B. *Macromolecules* **2000**, *33*, 5278.
(26) He, Y.; Lutz, T. R.; Ediger, M. D. *J. Chem. Phys.* **2003**, *119*, 9956.
(27) Graessley, W. W.; Krishnamoorti, R.; Balsara, N. P.; Fetters, L. J.; Lohse, D. L.; Schulz, D. N.; Sissano, J. A. *Macromolecules* **1993**, *26*, 1137.
(28) Kant, R.; Kumar, S. K.; Colby, R. H. *Macromolecules* **2003**, *36*, 10087.
(29) Meyer, A.; Dimeo, R. D.; Gehring, P. M.; Neumann, D. A. *Rev. Sci. Instrum.* **2003**, *74*, 2762.
(30) The IDL-based program can be found at http://www.ncnr.nist.giv/dave/.
(31) Williams, G.; Watts, D. C. *Trans. Faraday Soc.* **1970**, *66*, 80.
(32) Alegría, A.; Elizetxea, C.; Cendoya, I.; Colmenero, J. *Macromolecules* **1995**, *28*, 8819.
(33) Arbe, A.; Alegría, A.; Colmenero, J.; Hoffmann, S.; Willner, L.; Richter, D. *Macromolecules* **1999**, *32*, 7572.
(34) Min, B.; Qiu, X.; Ediger, M. D.; Pitsikalis, M.; Hadjichristidis, N. *Macromolecules* **2001**, *34*, 4466.
(35) Carlsson, P.; Zorn, R.; Andersson, D.; Farago, B.; Howells, W. S.; Börjesson, L. *J. Chem. Phys.* **2001**, *114*, 9645.
(36) Farago, B.; Arbe, A.; Colmenero, J.; Faust, R.; Buchenau, U.; Richter, D. *Phys. Rev. E* **2002**, *65*, 051803.
(37) Arbe, A.; Moral, A.; Alegría, A.; Colmenero, J.; Pyckhout-Hintzen, W.; Richter, D.; Farago, B.; Frick, B. *J. Chem. Phys.* **2002**, *117*, 1336.
(38) Arbe, A.; Colmenero, J.; Farago, B.; Monkenbusch, M.; Buchenau, U.; Richter, D. *Chem. Phys.* **2003**, *292*, 295.
(39) Bergman, R.; Alvarez, F.; Alegría, A.; Colmenero, J. *J. Noncryst. Solids* **1998**, *235*, 580.
(40) Moreno, A. J.; Alegría, A.; Colmenero, J.; Frick, B. *Macromolecules* **2001**, *34*, 4886.
(41) Arbe, A.; Richter, D.; Colmenero, J.; Farago, B. *Phys. Rev. E* **1996**, *54*, 3853.
(42) Colmenero, J.; Alvarez, F.; Arbe, A. *Phys. Rev. E* **2002**, *65*, 041804.
(43) Richter, D.; Monkenbusch, M.; Arbe, A.; Colmenero, J.; Farago, B.; Faust, R. *J. Phys.: Condens. Matter* **1999**, *11*, A297.
(44) Neelakantan, A.; Maranas, J. K. *J. Chem. Phys.* **2004**, *120*, 465.
(45) Colmenero, J.; Arbe, A.; Alegría, A.; Monkenbusch, M.; Richter, D. *J. Phys.: Condens. Matter* **1999**, *44*, A363.
(46) Colmenero, J.; Alegría, A.; Arbe, A.; Frick, B. *Phys. Rev. Lett.* **1992**, *69*, 478.
(47) Cicerone, M. T.; Ediger, M. D. *J. Chem. Phys.* **1996**, *104*, 7210.
(48) Donati, C.; Glotzer, S. C.; Poole, P. H. *Phys. Rev. Lett.* **1999**, *82*, 5064.
(49) Deschenes, L. A.; Vandenbout, D. A. *Science* **2001**, *292*, 255.
(50) Fytas, G.; Wang, C. H.; Fischer, E. W. *Macromolecules* **1988**, *21*, 2253.
(51) The use of the commercial products identified in this paper does not imply recommendation or endorsement by the National Institute of Standards and Technology, nor does it imply that the materials or equipment identified are necessarily the best available for the purpose.

MA0497355